Ceramics International 46 (2020) 2213–2219

Contents lists available at ScienceDirect

Ceramics International

journal homepage: www.elsevier.com/locate/ceramint

Electrocaloric properties of $Ba_{0.8}Sr_{0.2}Ti_{1-x}Zr_xO_3$ ($0 \leq x \leq 0.1$) system: The balance between the nature of the phase transition and phase coexistence

Keriman Şanlı, Umut Adem*

Department of Materials Science and Engineering, İzmir Institute of Technology, Urla, 35430, İzmir, Turkey

ARTICLE INFO

Keywords:
Electrocaloric effect
Barium titanate
Critical point
Diffuse phase transition
Polymorphic phase transition

ABSTRACT

We investigate the electrocaloric effect of $Ba_{0.8}Sr_{0.2}Ti_{1-x}Zr_xO_3$ ($0 \leq x \leq 0.1$) system by comparing the electrocaloric temperature change (ΔT) of different compositions belonging to the different regions of the phase diagram. We show that as the amount of Zr increases, electrocaloric temperature change initially decreases as the phase transition gets diffuse then increases again as the composition of the samples are located closer to the critical point where different ferroelectric phases coexist. Since the critical point is reached at relatively low Zr substitution levels (i.e. around $x = 0.07$), the phase transition doesn't get too diffuse and thefore the compositions between $x = 0$ and $x = 0.10$ (which contains higher Zr than the critical point composition) have comparable ΔT values. Electrocaloric efficiency of these compositions ($x = 0.03$, 0.05 and 0.07) is around 0.20 K mm/kV at 20 kV/cm. We discuss the results in terms of the balance between the nature of the phase transition and proximity to the critical point, based on the phase diagram.

1. Introduction

Electrocaloric effect is the temperature change induced by an electric field under adiabatic conditions in a dielectric material. After the discovery of large electrocaloric temperature change (ΔT) in $Pb_{0.95}Zr_{0.05}TiO_3$ thin films [1] and P(VDF-TrFE) [2] there has been renewed interest in the electrocaloric materials due to their potential for utilization in electrocaloric cooling applications. Electrocaloric cooling based on electrocaloric effect is one of the solid state cooling technology alternatives to conventional gas compression based cooling technology. It is potentially more efficient than conventional cooling and offers a hazardous gas-free, light, and a noise free cooler [3,4]. However, much larger electrocaloric temperature changes are necessary for the realization of the electrocaloric refrigeration. Additionally, since some of most promising electrocaloric ceramics contain environmentally hazardous Pb element, research is focused on developing electrocaloric properties of Pb-free ceramics. These Pb-free ceramic families include $BaTiO_3$, $Na_{0.5}Bi_{0.5}TiO_3$ [5,6], $K_{0.5}Na_{0.5}NbO_3$ based materials [7] as well as layered ferroelectrics such as Aurivilius [8] and tetragonal bronze [9] phases. More recently, defect engineering strategies are also being explored to increase ΔT [10–14].

Among Pb-free ferroelectrics, there have been quite a few studies on the electrocaloric effect of $BaTiO_3$ based materials. Largest ΔT values in $BaTiO_3$ based systems are observed for $BaTiO_3$ itself due to the sharpness of the ferroelectric phase transition however this large ΔT is preserved only in a narrow temperature range around Curie temperature due to the first order nature of the phase transition [15]. Substitution strategies focus on keeping a relatively large electrocaloric temperature change over a broader temperature range, making use of different mechanisms. Different substitution and co-substitution combinations have already been tried for $BaTiO_3$ based systems. Typical substitutions include Ca and Sr [16,17] for the A-site and Zr [18], Sn [19] and Hf [20] for the B-site, respectively. Doping at both A- and B-sites has been more commonly tried [21–26]. Bai et al. studied the electrocaloric effect of $Ba_{1-x}Sr_xTiO_3$ ceramics ($x = 0.2$–0.4). They showed that combination of the effects of the grain size and nature of the phase transition (first order like or diffuse) determines the optimum composition for the electrocaloric effect [17]. Li et al. studied $Ba_{0.9}Sr_{0.1}(Ti_{0.9}Zr_{0.1})_{0.95}Sn_{0.05}O_3$ ceramic. Such large amounts of Zr and Sn at the B-site induces relaxor ferroelectricity and diffuse phase transition. The presence of polar nanoregions facilitates polarization rotation and improves EC efficiency or strength, defined as the electrocaloric temperature change obtained per unit applied electric field ($\Delta T/\Delta E$) [27]. Similarly, Qi et al. started with $BaTi_{0.9}Sn_{0.1}O_3$ and replaced Ba with Sr, up to 8%. Phase transition temperature decreases towards room temperature by Sr doping at the A-site while the diffuse character of the transition is preserved. $\Delta T/\Delta E$ of the best Sr-doped composition was comparable to the $BaTi_{0.9}Sn_{0.1}O_3$ composition. Liu et al. studied the

* Corresponding author.
E-mail address: umutadem@iyte.edu.tr (U. Adem).

https://doi.org/10.1016/j.ceramint.2019.09.206
Received 24 August 2019; Received in revised form 18 September 2019; Accepted 20 September 2019
Available online 21 September 2019

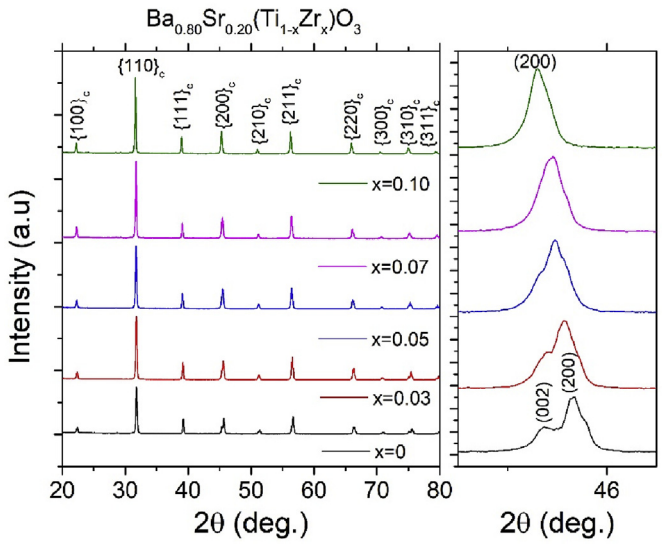

Fig. 1. XRD patterns for all compositions. The peaks are indexed using pseudocubic reflections of the perovskite structure. The panel in the right shows a close-up view of the region near 2θ = 45°.

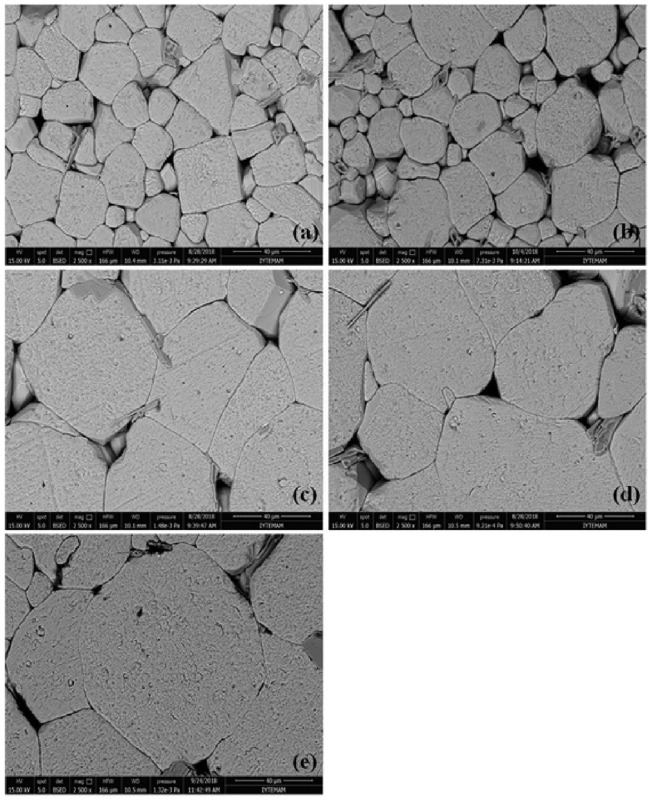

Fig. 2. SEM images for all compositions: (a) x = 0, (b) x = 0.03, (c)x = 0.05, (d) x = 0.07 and (e) x = 0.10.

effects of Spark Plasma Sintering (SPS) process and Mn doping on the electrocaloric properties of $Ba_{0.7}Sr_{0.3}TiO_3$ ceramics. They show that SPS process and Mn doping both help to increase the dielectric breakdown strength and thus ΔT [16]. Li et al. studied the electrocaloric effect of $BaHf_xTi_{1-x}O_3$ ceramics based on the phase diagram. They showed that for x = 0.11, at the critical point composition of the phase diagram where all ferroelectric phases (tetragonal, orthorhombic, rhombohedral) of $BaTiO_3$ meet, a large ΔT as well as large electrocaloric efficiency ΔT/ΔE can be obtained due to the large entropy change arising

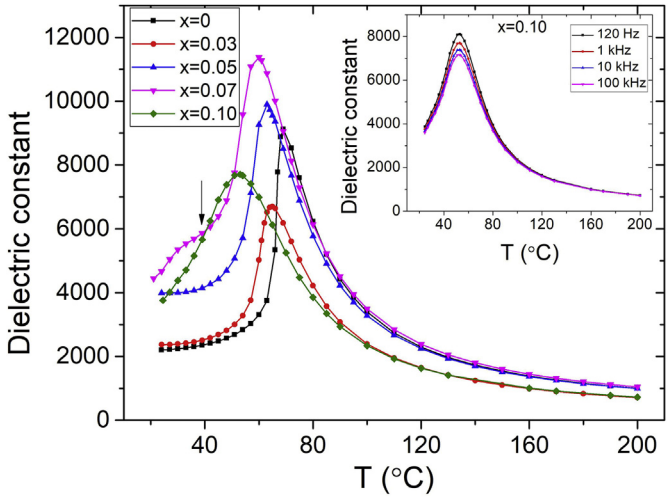

Fig. 3. Dielectric constant of all compositions as a function of temperature, measured at 1 kHz. In the inset, temperature dependence of the dielectric constant of x = 0.10 sample at different frequencies is shown.

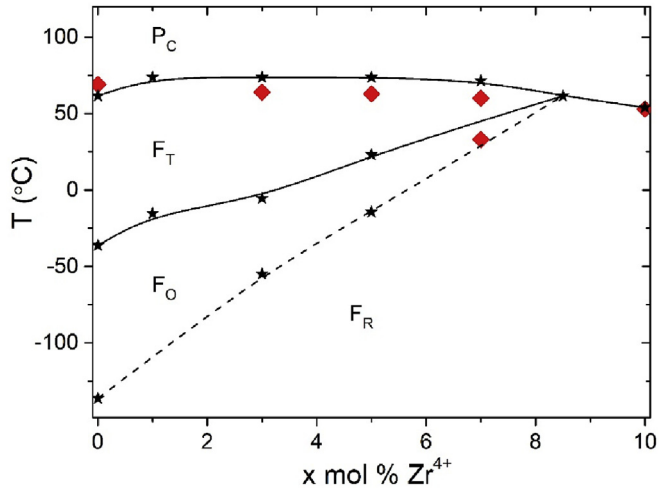

Fig. 4. Phase diagram of $Ba_{0.8}Sr_{0.2}Ti_{1-x}Zr_xO_3$ ($0 \le x \le 0.1$) ceramics. Star symbols are reproduced from Szymczak et al. [28] while diamond symbols represent transition temperatures measured in this study. F_R, F_O and F_T represent ferroelectric rhombohedral, orthorhombic and tetragonal phases, where P_C represent paraelectric cubic phase of $BaTiO_3$.

from the coexistence of many ferroelectric phases and availability of many polarization directions, respectively [20].

Here, based on the phase diagram reported in Ref. [28], we investigate the correlation between the location of the material composition on the phase diagram and the physical mechanisms controlling the electrocaloric temperature change, ΔT of $Ba_{0.8}Sr_{0.2}Ti_{1-x}Zr_xO_3$ ($0 \le x \le 0.1$) system in detail. Such comprehensive analysis of ΔT performed by studying the correlation between the location of composition on the phase diagram and corresponding physical mechanisms has only been reported in a few studies on B-site Hf substituted $BaTiO_3$ compositions [20,21].

2. Experimental

$Ba_{0.8}Sr_{0.2}Ti_{1-x}Zr_xO_3$ ($0 \le x \le 0.1$) compositions were synthesized using solid state synthesis. Stoichiometric amounts of precursors $BaCO_3$ (> 99.9%), $SrCO_3$ (> 99.9%), TiO_2 (> 99.9%) and ZrO_2 (> 99.9%) were mixed using ball milling in nalgene bottles using YSZ (yttria stabilized zirconia) balls with ethanol. Dried powder were calcined at

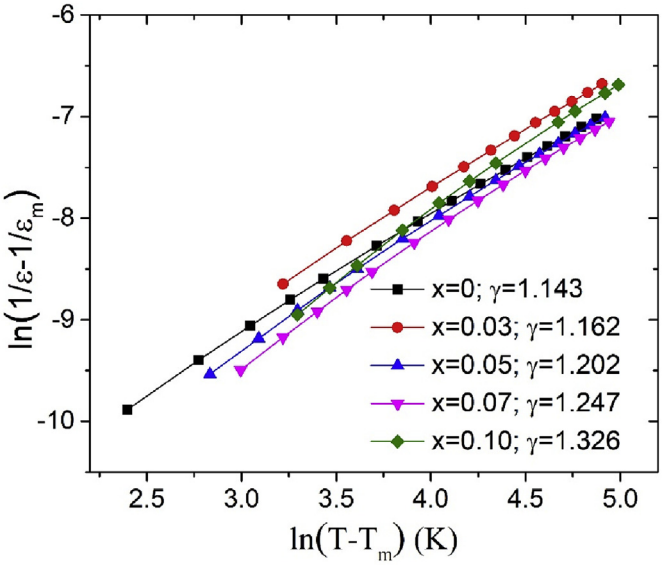

Fig. 5. $\ln(1/\varepsilon\text{-}1/\varepsilon_m)$ as a function of $\ln(T\text{-}T_m)$ for all compositions.

1100 °C for 4 h. Calcined powder were mixed with 2 wt % polyvinyl alcohol (PVA) for 8 h and pelletized after drying. Resulting pellets were sintered at 1400 °C for 4 h in Pt lined alumina crucibles after binder burnout at 600 °C for 4 h. Pellets used for electrical measurements were less than 1 mm thick. Ag epoxy was used to form the electrodes. Density of the samples was measured using an Archimedes setup. X-ray diffraction (XRD) measurements were done using a Panalytical X'Pro Instrument with Cu K_α source. Microstructure of the pellets were examined by using a Scanning Electron Microscope (SEM, Philips XL 30S FEG). Dielectric measurements were done between room temperature and 200 °C using an Agilent E4980AL LCR Meter between 120 Hz and 100 kHz. Ferroelectric hysteresis loops of the samples were collected using a Aixacct TF Analyzer 1000 in the same temperature range as in the dielectric measurements.

3. Results and discussion

3.1. Microstructural characterization

In Fig. 1, XRD patterns of all compositions collected at room temperature are shown. All peaks belong to the perovskite structure. As the amount of Zr increases, XRD peaks shift towards lower angles due to the incorporation of larger Zr^{4+} ions (0.72 Å) to the Ti^{4+} (0.605 Å) sites. A close-up look to the 45° peaks given in the right panel of Fig. 1 shows clear tetragonal splitting for undoped $Ba_{0.8}Sr_{0.2}TiO_3$ and $Ba_{0.8}Sr_{0.2}Ti_{0.97}Zr_{0.03}O_3$ compositions. The splitting can still be noticed for x = 0.05 composition, whereas for x = 0.07 and x = 0.10 compositions no splitting can be observed. Judging from the lack of tetragonal splitting and the location of the compositions on the phase diagram introduced in Fig. 4, at room temperature x = 0.07 likely consists of a mixture of ferroelectric orthorhombic and rhombohedral phases while x = 0.10 is rhombohedral. In Fig. 2, SEM images taken at 2500 magnification are shown for all compositions. All compositions show relatively dense microstructures. Grain size increases with Zr substitution. Grain sizes are approximately 30, 36, 68, 77 and 96 μm for x = 0, 0.03, 0.05, 0.07 and 0.10 compositions, respectively.

3.2. Dielectric measurements

Fig. 3 shows temperature dependence of the dielectric constant for all compositions at 1 kHz. In x = 0 sample, a relatively sharp dielectric peak occurs at the Curie temperature of 69 °C. With increasing Zr content, dielectric peak progressively moves to lower temperatures and becomes broader. Peak value of the dielectric constant initially decreases going from x = 0 to x = 0.03 composition but then increases again to become maximum for x = 0.07 composition and decreases again for x = 0.10 composition. In the inset, dielectric constant of x = 0.10 is plotted against temperature at different frequencies. There is weak frequency dependence however peak temperature does not shift with frequency suggesting that the phase transition has diffuse rather than relaxor character. Temperatures of the dielectric peaks as well as the temperature of the additional anomaly corresponding to the

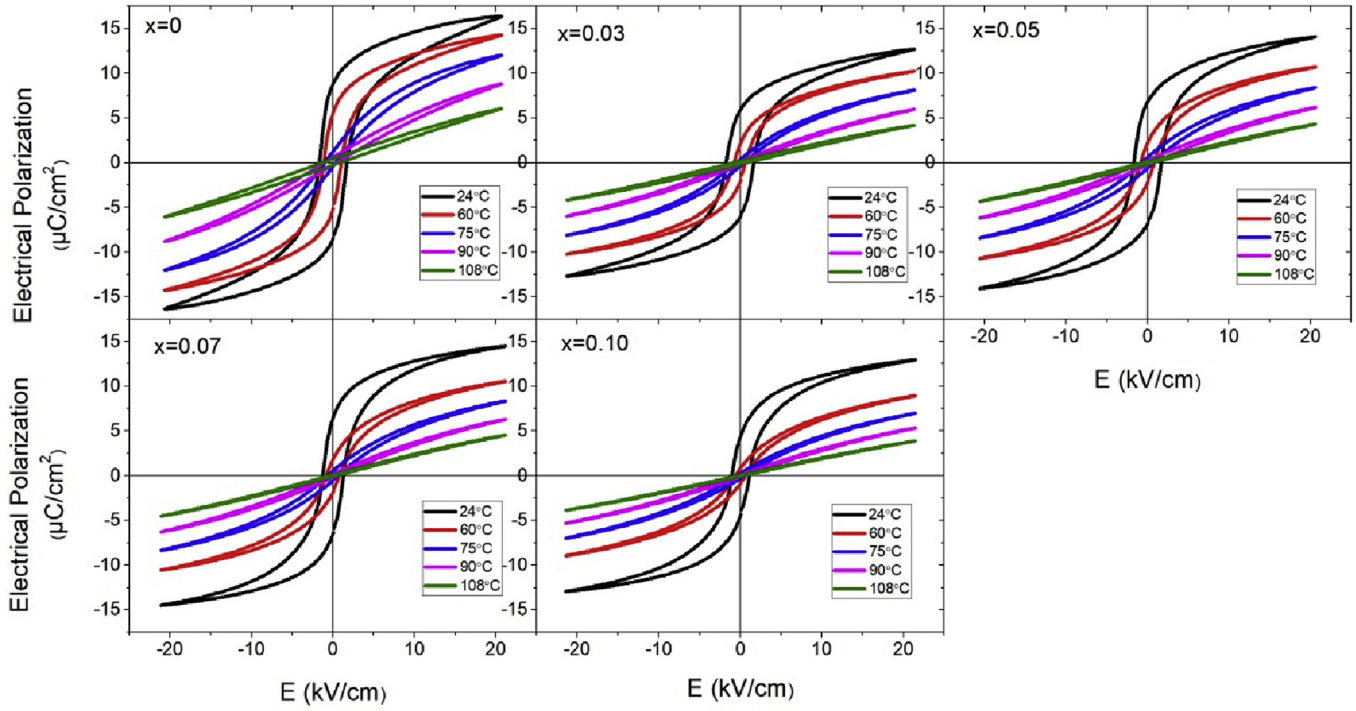

Fig. 6. Temperature dependence of the electrical polarization of $Ba_{0.8}Sr_{0.2}Ti_{1-x}Zr_xO_3$ ($0 \le x \le 0.1$) ceramics, measured at 1 kHz.

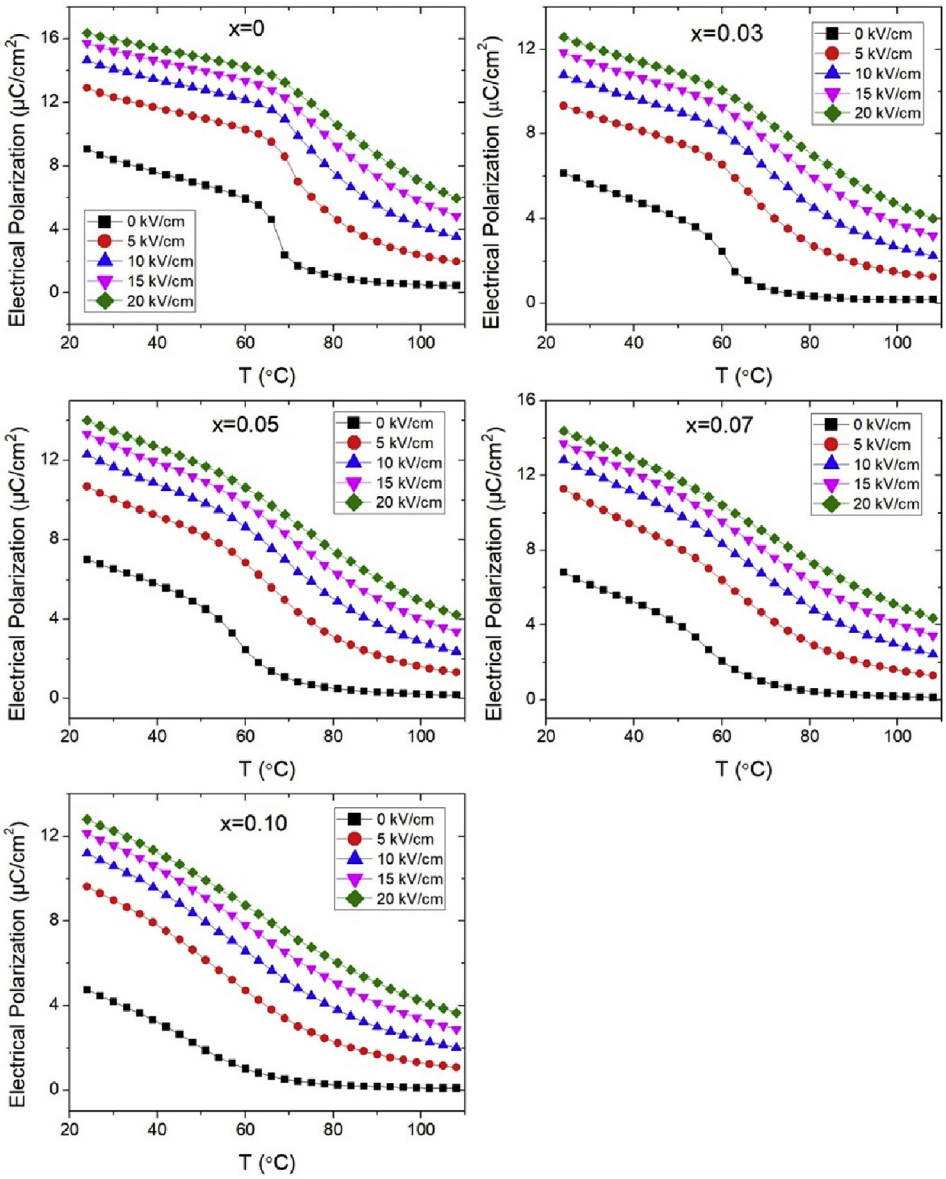

Fig. 7. Electrical polarization as a function temperature of all compositions, at different electric field values.

polymorphic phase transition (orthorhombic-tetragonal transition, indicated by an arrow in Fig. 3) for x = 0.07 sample are added to the phase diagram published by Szymczak et al. [28] and shown in Fig. 4. The transition temperatures obtained by us slightly differ from those measured by Szymczak et al. In order to evaluate the diffuseness level of the phase transition, modified Curie-Weiss law is used:

$$\frac{1}{\varepsilon} - \frac{1}{\varepsilon_m} = \frac{(T - T_m)^{\gamma}}{C'} \quad (1)$$

In this equation, ε_m corresponds to the maximum dielectric constant, T_m is the temperature at which ε_m is observed and γ and C' are constants. Diffuseness coefficient γ for each composition is calculated from the fits to the modified Curie-Weiss law as shown in Fig. 5. $\gamma = 1$ describes normal ferroelectric behaviour while $\gamma = 2$ implies relaxor ferroelectric behaviour [29]. γ value is obtained as 1.143, 1.162, 1.202, 1.247 and 1.326 for x = 0.00, 0.03, 0.05, 0.07 and 0.10, respectively. As expected, γ increases with Zr substitution; however, even for x = 0.10 composition, it does not approach 2, therefore phase transition has diffuse rather than relaxor ferroelectric character. This conclusion is in agreement with the frequency independent dielectric peak position shown in the inset of Fig. 3.

3.3. Electrocaloric effect

Ferroelectric hysteresis loops measured at different temperatures and 1 Hz for all compositions are shown in Fig. 6. At room temperature, remanent polarization (P_r) decreases abruptly going from x = 0 to x = 0.03 but then increases again for x = 0.05 and x = 0.07 compositions before decreasing again for x = 0.10 composition. Considering the location of each composition on the phase diagram, their crystal structures and grain sizes, we explain the trends in remanent polarization with composition. Zr substitution decreases tetragonality [30] which might explain the decrease in the remanent polarization going from x = 0 to x = 0.03 composition. x = 0.05 and x = 0.07 samples are located closer to the critical point where more polarization directions are active and grain sizes of these compositions are larger, both accounting for the increase in P_r. Above the Curie temperature of each composition the loops become linear as the paraelectric phase becomes stable.

To calculate the electrocaloric temperature change, ΔT, of each composition, indirect method based on Maxwell's equations was used:

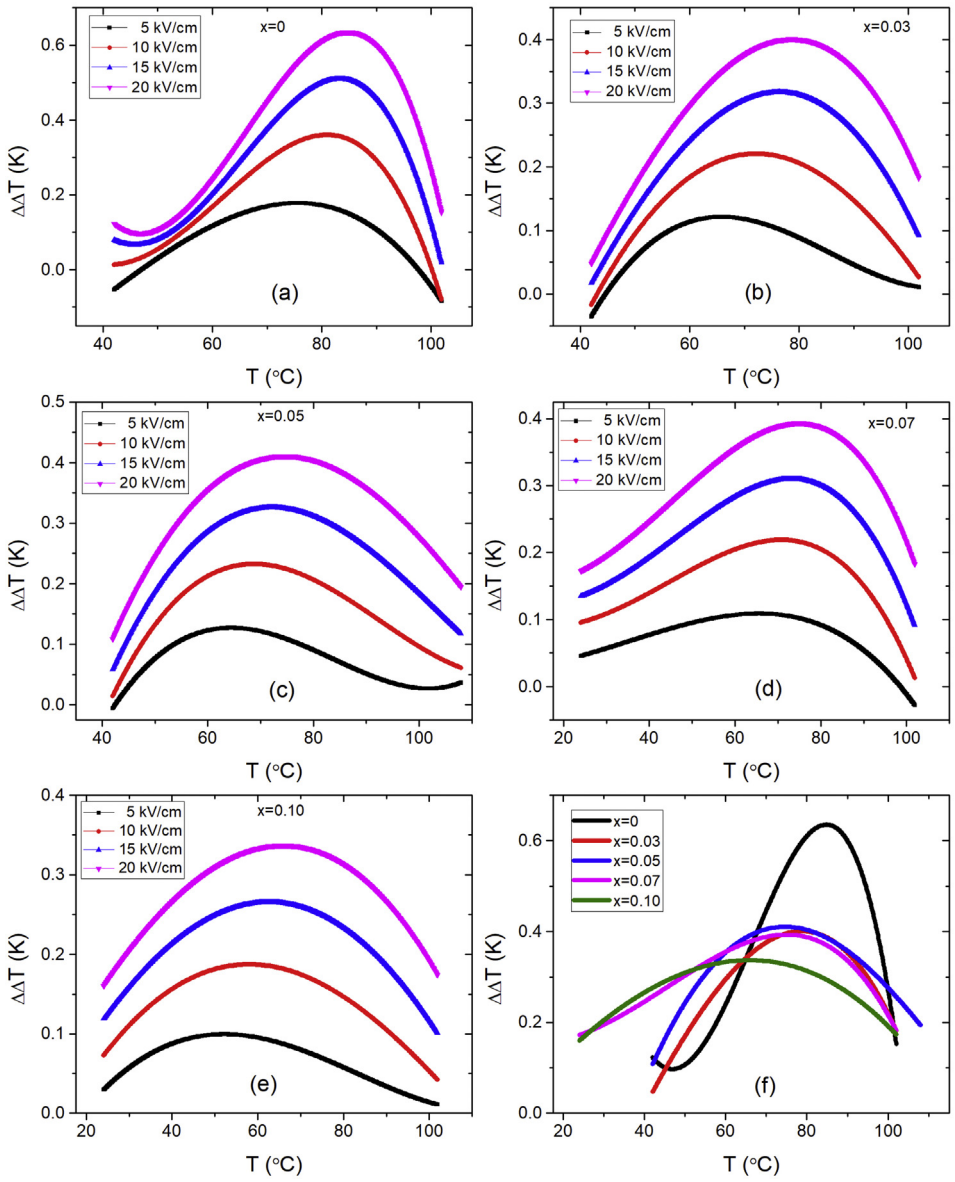

Fig. 8. (a)-(e) Electrocaloric temperature change (ΔT) under 0, 5, 10, 15 and 20 kV/cm for all compositions and (f) Comparision of ΔT of all compositions under 20 kV/cm.

Table 1
Comparison of electrocaloric properties of $Ba_{0.8}Sr_{0.2}Ti_{1-x}Zr_xO_3$ ($0 \leq x \leq 0.1$) ceramics with other $BaTiO_3$ based ceramics in the literature.

Material	Form	T_C or T_m(K)	ΔT (K)	ΔE (kV/cm)	ΔT/ΔE (K.mm/kV)	Method	Ref.
$BaTiO_3$	single crystal	402	0.9	12	0.75	Direct	[15]
$BaTiO_3$	ceramic	398	1.1	20	0.56	Indirect	[32]
$Ba_{0.65}Sr_{0.35}TiO_3$	ceramic	296	0.42	20	0.21	Indirect	[17]
$BaTi_{0.89}Hf_{0.11}O_3$	ceramic	343	0.35	10	0.35	Indirect	[20]
$Ba_{0.9}Sr_{0.1}(Ti_{0.9}Zr_{0.1})_{0.95}Sn_{0.05}O_3$	ceramic	303	0.22	7.5	0.29	Direct	[27]
$Ba_{0.87}Ca_{0.13}(Ti_{0.87}Hf_{0.13})O_3$	ceramic	≈323	0.30	10	0.30	Direct	[21]
$Ba_{0.7}Sr_{0.3}Ti_{0.997}Mn_{0.003}O_3$	Ceramic	308	1.63	70	0.233	Indirect	[16]
x = 0	ceramic	351	0.62	20	0.31	Indirect	This work
x = 0.03	ceramic	351	0.42	20	0.21	Indirect	This work
x = 0.05	ceramic	351	0.43	20	0.215	Indirect	This work
x = 0.07	ceramic	351	0.40	20	0.20	Indirect	This work
x = 0.10	ceramic	342	0.35	20	0.175	Indirect	This work

$$\Delta T = -\frac{1}{\rho}\int_{E_1}^{E_2}\frac{T}{c_p}\left(\frac{\partial P}{\partial T}\right)_E dE \quad (2)$$

Here, P is the electrical polarization, T is the temperature, ρ is the density, c_p is the specific heat and E_1, E_2 are initial and final electric fields, respectively. In the calculation, E_1 was taken as 0 and various E_2 values are used to observe the change of ΔT with increasing E. Measured ρ values were put in for the calculation (5.23, 5.33, 5.36, 5.35

and 5.33 g/cm^3 for x = 0, 0.03, 0.05, 0.07 and 0.10, respectively). And a constant c_p value of 0.5 J g^{-1} K^{-1} was assumed for all compositions, which is slightly larger than what has been previously reported in Sr and Zr co-substituted $BaTiO_3$ compositions [27].

In order to obtain $\left(\frac{\partial P}{\partial T}\right)_E$, first, polarization values at different fixed electric fields as a function of temperature are extracted from the 2nd quadrant of the hysteresis loops. Then, these P(T) curves, -which are shown at different electric field values in Fig. 7- are fitted by using a 4th order polynomial and the derivative of the resulting curve is taken.

Calculated ΔT of all compositions at different temperatures are given in Fig. 8. Corresponding to the sudden drop in the polarization of x = 0 composition around the Curie temperature, a sharp increase is observed in ΔT. ΔT of this composition exceeds 0.6 K at 20 kV/cm. As Zr content increases, maximum ΔT decreases initially while getting broader for x = 0.03 composition and then increases again for x = 0.05. x = 0.07 composition, which is the closest composition to the critical point has a slightly lower ΔT peak than x = 0.05 and even x = 0.03, however is also broader. The difference in ΔT of these compositions, x = 0.03, 0.05 and 0.07 is quite small. Finally, ΔT peak of x = 0.10 sample is the lowest in magnitude and the broadest of all compositions. Electrocaloric efficiency of all compositions are listed in Table 1 together with the literature values of $BaTiO_3$ based compositions. As can be seen from the Table, the values obtained in this study are slightly lower but also comparable with the literature values.

The compositional trend in ΔT can be understood by considering the combined effects of the location of the composition in the phase diagram (proximity to the critical point or phase boundaries), grain size and the nature of the phase transition (is also related with the location of the composition in the phase diagram). As expected, x = 0 material shows the largest ΔT in a narrow T range due to the 1st order like nature of the phase transition. ΔT trend in our Zr-substituted compositions described above is different from the literature results. In $BaHf_xTi_{1-x}O_3$ [20] and $Ba_{0.87}Ca_{0.13}Ti_{0.87}Hf_{0.13}O_3$ [21], ΔT becomes maximum at the composition closest to the critical point, where all ferroelectric phases of $BaTiO_3$ meet and increase the entropy change. In our case, critical point composition x = 0.07 has slightly lower ΔT than x = 0.05 and 0.03. This difference might originate from the fact that in our case, even for x = 0.07 composition closest to the critical (invariant) point, the phase transition is not very diffuse (γ = 1.247 for our x = 0.07 sample compared to γ = 1.59 of $Ba_{0.87}Ca_{0.13}Ti_{0.87}Hf_{0.13}O_3$ [21]), and slightly less diffuse nature of the phase transition of x = 0.03 and x = 0.05 samples might counteract the increase in ΔT of x = 0.07 due to the multiphase coexistence effect. It is known that grain size is another factor affecting ΔT [31] and we can expect that it also contributes here since grain sizes of x = 0.05 and x = 0.07 compositions are significantly larger than those of x = 0 and x = 0.03. However, a systematic study is needed to pinpoint its effect here. Last parameter that should be considered is the specific heat. We assumed a constant specific heat value in our calculations. However, specific heat obviously changes with the composition and it is reported that at the critical point compositions, it becomes smaller than undoped composition [20,21]. This also implies a larger ΔT than we calculated for x = 0.07. Alternatively, it might be also possible that x = 0.07 is slightly off from the critical point composition in our case. Another important difference of our results compared to other studies where ΔT was engineered based on the phase diagram [20,21], is the fact that critical point is reached with less doping at the B-site (e.g. ~7 mol % vs 11 mol % [20]). This might partially explain the lower diffuseness coefficients in our case. Even though the phase transition does not become very diffuse even at x = 0.10 composition, ΔT peaks become relatively broad while the peak value remains relatively large up to x = 0.07. We suggest that x = 0.07 composition can be chosen as the optimum composition for cooling applications -despite the slightly lower ΔT compared to x = 0.05 and x = 0.03- since a relatively large ΔT is kept over the widest temperature range.

4. Conclusions

In conclusion, we have studied the electrocaloric properties of $Ba_{0.8}Sr_{0.2}Ti_{1-x}Zr_xO_3$ ($0 \le x \le 0.1$) system using the indirect method. We observed that Zr substitution makes the ferroelectric phase transition diffuse but does not cause relaxor ferroelectricity even for x = 0.10 composition. As the critical point is reached at relatively low Zr substitution levels (i.e. around x = 0.07), the phase transition doesn't get too diffuse and thefore the compositions between x = 0 and x = 0.10 (which contains higher Zr than the critical point composition) have comparable ΔT values. Since even at the critical point composition (x = 0.07), diffuseness coefficient γ is small, having a relatively sharp phase transition and being located close to the critical point are both effective for controlling ΔT of x = 0.03, 0.05 and 0.07 compositions and the balance between these two factors determine ΔT. Comparable and relatively large electrocaloric efficiency values of around 0.20 K mm/kV at 20 kV/cm are obtained for these three compositions.

Declaration of interests

The authors declare that they have no known competing financial interests or personal relationships that could have appeared to influence the work reported in this paper.

Acknowledgements

This work is supported by Career Grant Program of the Scientific and Technological Research Council of Turkey (TUBITAK) with the project number 315M241. We acknowledge IZTECH Centre for Materials Research for the use of XRD and SEM instruments. The authors also thank Tuğçe Demirtay for her help with the experiments and useful discussions.

References

[1] A.S. Mischenko, Q. Zhang, J.F. Scott, R.W. Whatmore, N.D. Mathur, Giant electrocaloric effect in thin-film $PbZr_{0.95}Ti_{0.05}O_3$, Science 311 (2006) 1270–1271.
[2] B. Neese, B.J. Chu, S.G. Lu, Y. Wang, E. Furman, Q.M. Zhang, Large electrocaloric effect in ferroelectric polymers near room temperature, Science 321 (2008) 821–823.
[3] C. Aprea, A. Greco, A. Maiorino, C. Masselli, Solid-state refrigeration: a comparison of the energy performances of caloric materials operating in an active caloric regenerator, Energy 165 (2018) 439–455.
[4] A. Greco, C. Aprea, A. Maiorino, C. Masselli, A review of the state of the art of solid-state caloric cooling processes at room-temperature before 2019, Int. J. Refrig. 106 (2019) 66–88.
[5] W.P. Cao, W.L. Li, D. Xu, Y.F. Hou, W. Wang, W.D. Fei, Enhanced electrocaloric effect in lead-free NBT-based ceramics, Ceram. Int. 40 (2014) 9273–9278.
[6] F. Le Goupil, J. Bennett, A.K. Axelsson, M. Valant, A. Berenov, A.J. Bell, T.P. Comyn, N.M. Alford, Electrocaloric enhancement near the morphotropic phase boundary in lead-free NBT-KBT ceramics, Appl. Phys. Lett. 107 (2015) 172903.
[7] J. Koruza, B. Rozic, G. Cordoyiannis, B. Malic, Z. Kutnjak, Large electrocaloric effect in lead-free $K_{0.5}Na_{0.5}NbO_3$-$SrTiO_3$ ceramics, Appl. Phys. Lett. 106 (2015) 202905.
[8] A.-K. Axelsson, F. Le Goupil, M. Valant, N.M. Alford, Electrocaloric effect in lead-free Aurivillius relaxor ferroelectric ceramics, Acta Mater. 124 (2017) 120–126.
[9] F. Le Goupil, A.-K. Axelsson, L.J. Dunne, M. Valant, G. Manos, T. Lukasiewicz, J. Dec, A. Berenov, N. Alford, Anisotropy of the electrocaloric effect in lead-free relaxor ferroelectrics, Adv. Energy Mater. 4 (2014) 1301688.
[10] C.M. Guvenc, U. Adem, Influence of aging on electrocaloric effect in Li+ doped $BaTiO_3$ ceramics, J. Alloy. Comp. 791 (2019) 674–680.
[11] M. Wu, Q.S. Zhu, J.T. Li, D.S. Song, H.H. Wu, M.Y. Guo, J.H. Gao, Y. Bai, Y.J. Feng, S.J. Pennycook, X.J. Lou, Electrocaloric effect in ferroelectric ceramics with point defects, Appl. Phys. Lett. 114 (2019) 142901.
[12] H.M. Qiao, C. He, F.P. Zhuo, Z.J. Wang, X.Z. Li, Y. Liu, X.F. Long, Modulation of electrocaloric effect and nanodomain structure in Mn-doped $Pb(In_{0.5}Nb_{0.5})O_3$-$PbTiO_3$ ceramics, Ceram. Int. 44 (2018) 20417–20426.
[13] M. Wu, D.S. Song, G. Vats, S.C. Ning, M.Y. Guo, D.W. Zhang, D.Q. Xue, S.J. Pennycook, X.J. Lou, Defect-controlled electrocaloric effect in $PbZrO_3$ thin films, J. Mater. Chem. C 6 (2018) 10332–10340.
[14] T.D. Zhang, W.L. Li, Y.F. Hou, Y. Yu, W.P. Cao, Y. Feng, W.D. Fei, Positive/negative electrocaloric effect induced by defect dipoles in PZT ferroelectric bilayer thin films, RSC Adv. 6 (2016) 71934–71939.
[15] X. Moya, E. Stern-Taulats, S. Crossley, D. Gonzalez-Alonso, S. Kar-Narayan, A. Planes, L. Manosa, N.D. Mathur, Giant electrocaloric strength in single-crystal $BaTiO_3$, Adv. Mater. 25 (2013) 1360–1365.

[16] X.Q. Liu, T.T. Chen, M.S. Fu, Y.J. Wu, X.M. Chen, Electrocaloric effects in spark plasma sintered $Ba_{0.7}Sr_{0.3}TiO_3$-based ceramics: effects of domain sizes and phase constitution, Ceram. Int. 40 (2014) 11269–11276.
[17] Y. Bai, X. Han, K. Ding, L.J. Qiao, Combined effects of diffuse phase transition and microstructure on the electrocaloric effect in $Ba_{1-x}Sr_xTiO_3$ ceramics, Appl. Phys. Lett. 103 (2013) 162902.
[18] X.-S. Qian, H.-J. Ye, Y.-T. Zhang, H. Gu, X. Li, C.A. Randall, Q.M. Zhang, Giant electrocaloric response over a broad temperature range in modified $BaTiO_3$ ceramics, Adv. Funct. Mater. 24 (2014) 1300–1305.
[19] Z.D. Luo, D.W. Zhang, Y. Liu, D. Zhou, Y.G. Yao, C.Q. Liu, B. Dkhil, X.B. Ren, X.J. Lou, Enhanced electrocaloric effect in lead-free $BaTi_{1-x}Sn_xO_3$ ceramics near room temperature, Appl. Phys. Lett. 105 (2014) 102904.
[20] J.N. Li, D.W. Zhang, S.Q. Qin, T.Y. Li, M. Wu, D. Wang, Y. Bai, X.J. Lou, Large room-temperature electrocaloric effect in lead-free $BaHf_xTi_{1-x}O_3$ ceramics under low electric field, Acta Mater. 115 (2016) 58–67.
[21] L. Zhao, X.Q. Ke, Z.J. Zhou, X.Q. Liao, J.J. Li, Y. Wang, M. Wu, T.Y. Li, Y. Bai, X.B. Ren, Large electrocaloric effect over a wide temperature range in $BaTiO_3$-modified lead-free ceramics, J. Mater. Chem. C 7 (2019) 1353–1358.
[22] X.J. Wang, J.G. Wu, B. Dkhil, C.L. Zhao, T.Y. Li, W. Li, X.J. Lou, Large electrocaloric strength and broad electrocaloric temperature span in lead-free $Ba_{0.85}Ca_{0.15}Ti_{1-x}Hf_xO_3$ ceramics, RSC Adv. 7 (2017) 5813–5820.
[23] B. Asbani, J.L. Dellis, A. Lahmar, M. Courty, M. Amjoud, Y. Gagou, K. Djellab, D. Mezzane, Z. Kutnjak, M. El Marssi, Lead-free $Ba_{0.8}Ca_{0.2}ZrxTi_{1-x}O_3$ ceramics with large electrocaloric effect, Appl. Phys. Lett. 106 (2015) 042902.
[24] S. Qi, G. Zhang, L. Duan, T. Zeng, J. Cao, Electrocaloric effect in Pb-free Sr-doped $BaTi_{0.9}Sn_{0.1}O_3$ ceramics, Mater. Res. Bull. 91 (2017) 31–35.
[25] H. Kaddoussi, Y. Gagou, A. Lahmar, J. Belhadi, B. Allouche, J.L. Dellis, M. Courty, H. Khemakhem, M. El Marssi, Room temperature electro-caloric effect in lead-free $Ba(Zr_{0.1}Ti_{0.9})_{1-x}Sn_xO_3$ (x = 0, x = 0.075) ceramics, Solid State Commun. 201 (2015) 64–67.
[26] H. Kaddoussi, A. Lahmar, Y. Gagou, B. Asbani, J.L. Dellis, G. Cordoyiannis, B. Allouche, H. Khemakhem, Z. Kutnjak, E.M. Marssi, Indirect and direct electro-caloric measurements of $(Ba_{1-x}Ca_x)(Zr_{0.1}Ti_{0.9})O3$ ceramics (x = 0.05, x = 0.20), J. Alloy. Comp. 667 (2016) 198–203.
[27] T.Y. Li, X.Y. Liu, S. Shi, Y.H. Yin, H.F. Li, Q.Y. Wang, Y.L. Zhang, J.H. Bian, S.S. Rajput, C.B. Long, B.L. Peng, Y. Bai, Y.Z. Wang, X.J. Lou, Large electrocaloric efficiency over a broad temperature span in lead-free $BaTiO_3$-based ceramics near room temperature, Appl. Phys. Lett. 111 (2017) 202902.
[28] L. Szymczak, M. Adamczyk, M. Pawelczyk, Dielectric and pyroelectric properties of Zr-doped $(Ba_{0.8}Sr_{0.2})TiO_3$ Ceramics, Arch. Metall. Mater. 54 (2009) 943–949.
[29] X. Zhang, L. Wu, S. Gao, J.Q. Liu, B. Xu, Y.D. Xia, J. Yin, Z.G. Liu, Large electro-caloric effect in $Ba(Ti_{1-x}Sn_x)O_3$ ceramics over a broad temperature region, AIP Adv. 5 (2015) 047134.
[30] S.J. Kuang, X.G. Tang, L.Y. Li, Y.P. Jiang, Q.X. Liu, Influence of Zr dopant on the dielectric properties and Curie temperatures of $Ba(Zr_xTi_{1-x})O_3$ ($0 \leq x \leq 0.12$) ceramics, Scr. Mater. 61 (2009) 68–71.
[31] M. Vrabelj, H. Ursic, Z. Kutnjak, B. Rozic, S. Drnovsek, A. Bencan, V. Bobnar, L. Fulanovic, B. Malic, Large electrocaloric effect in grain-size-engineered 0.9Pb$(Mg_{1/3}Nb_{2/3})O_3$-0.1$PbTiO_3$, J. Eur. Ceram. Soc. 36 (2016) 75–80.
[32] X.C. Ren, W.L. Nie, Y. Bai, L.J. Qiao, Effect of sintering temperature and oxygen atmosphere on electrocaloric effect of $BaTiO_3$ ceramics, Eur. Phys. J. B 88 (2015) 232.